^{1}H NMR Spectroscopy of Imidazole Ligands in Paramagnetic Ferric and Ferrous Complexes and Clusters. Relevance to Non-Heme Proteins

Feng-Jung Wu and Donald M. Kurtz, Jr.*

Contribution from the Department of Chemistry, University of Georgia, Athens, Georgia 30602.
Received December 23, 1988

Abstract: To provide an overview of the ^{1}H NMR behavior expected for imidazole ligands to paramagnetic non-heme iron, a set of ferric and ferrous imidazole complexes and a new set of binuclear and trinuclear clusters have been examined. For the effectively octahedral high-spin ferrous hexakis(imidazole) complexes, the isotropic shifts at 300 K are exclusively contact in origin. For these complexes, σ spin delocalization dominates, and the order of downfield isotropic shifts at 300 K is N(1)-H > 5-H > 4-H > 2-H > N-CH_3 $\gtrsim$ 5-CH_3. Anti-Curie behavior of the 4-H resonance at low temperature is attributed to a dipolar contribution in a lower symmetry structure. For low-spin Fe(III) direct π spin delocalization leads to upfield contact contributions for imidazole ring protons and downfield contact contributions for ring methyls. In the case of low-spin $[Fe(TICOH)_2]^{3+}$ (TICOH = tris(*N*-methylimidazol-2-yl)hydroxymethane), dipolar contributions were quantitatively separated from the contact contributions. From this separation the orientation of the imidazole rings with respect to the principal magnetic axis was determined. For imidazole ligands in high-spin ferric clusters, σ spin delocalization leads to exclusively downfield isotropic shifts, usually in the order N(1)-H > 4-H > 5-H > 2-H > 5-CH_3 $\gtrsim$ N-CH_3. The imidazole ligand 2-H and 4-H were observable only for the trinuclear "basic iron carboxylate" clusters, due to an unusually short T_{1e}. The results indicate that the histidyl ligand β-CH_2 should be observable well downfield of 10 ppm for magnetically uncoupled high-spin ferric sites and upfield of 9 ppm for $-J \gtrsim 30$ cm^{-1}. The imidazole N(1)-H (19.2 and 15.1 ppm) and acetate methyl (10.2 ppm) resonances of the diiron(III) complex, $[Fe_2O(O_2CMe)_2(TIP)_2]^{2+}$ (TIP = tris(imidazol-2-yl)phosphine), together confirm the presence of a μ-oxo rather than μ-hydroxo bridge in oxy- and methemerythrin; for azidomethemerythrin the NMR data indicate 62 cm^{-1} $\lesssim -J \lesssim$ 122 cm^{-1}. The 4.1 ppm separation between the two N(1)-H resonances of $[Fe_2O(O_2CMe)_2(TIP)_2]^{2+}$ reflects the μ-oxo trans effect, which appears to be smaller than that in hemerythrin. For the mixed-valent "basic iron carboxylate" clusters, valence delocalization allows the upfield dipolar contributions to the isotropic shifts to be understood in terms of distances and angles of the ligand protons with respect to magnetic axes of the *cluster*.

Imidazole ligands to non-heme iron are either known or suspected to occur in a significant number of proteins.[1] Ferrous and ferric oxidation states, high- or low-spin states, and mono- or binuclear sites are all represented. The work of La Mar and co-workers has established ^{1}H NMR as a useful probe of the structural and magnetic environment of imidazole ligands in heme proteins.[3] More recently, ^{1}H NMR of imidazole ligands has been shown to be a useful structural and magnetic probe of the non-heme iron sites in uteroferrin,[4] hemerythrin,[5] and catechol 1,2-dioxygenase.[2c] ^{1}H NMR of synthetic complexes constitutes an essential adjunct to interpretation of the protein spectra. Examinations of non-heme iron-imidazole complexes by ^{1}H NMR have been limited mostly to imidazole adducts of high-spin ferric and ferrous salen[2c,4,6] or closely related complexes. To our knowledge there have been no ^{1}H NMR studies of imidazole (excluding benzimidazole) ligands in polynuclear iron complexes, and only a few ^{1}H NMR spectra of non-heme low-spin ferric imidazole

Chart I

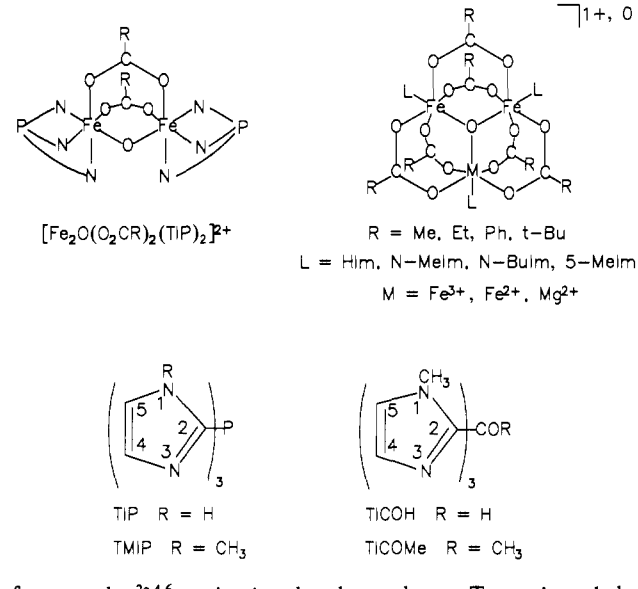

(1) These proteins include transferrin and lactoferrin,[2a] bacterial superoxide dismutase,[2b] catechol dioxygenases,[2c,d] the bacterial photosynthetic reaction center,[2e] hemerythrin,[2f] uteroferrin and purple acid phosphatases,[2f] ribonucleotide reductase,[2f] Rieske iron-sulfur proteins,[2f] and rubrerythrin.[2g]

(2) (a) Swope, S. K.; Chasteen, N. D.; Weber, K. E.; Harris, D. C. *J. Am. Chem. Soc.* **1988**, *110*, 3835-3840. (b) Carlioz, A.; Ludwig, M. L.; Stallings, W. C.; Fee, J. A.; Steinman, H. M. *J. Biol. Chem.* **1988**, *263*, 1555-1562. (c) Que, L., Jr.; Lauffer, R. B.; Lynch, J. B.; Murch, B. P.; Pyrz, J. W. *J. Am. Chem. Soc.* **1987**, *109*, 5381-5385. (d) Ohlendorf, D. H.; Lipscomb, J. D.; Weber, P. C. *Nature* **1988**, *336*, 403-405. (e) Deisenhofer, J.; Epp, O.; Miki, K.; Huber, R.; Michel, H. *Nature* **1985**, *318*, 618-624. (f) *Metal Clusters in Proteins*; ACS Symposium Series No. 372; Que, L., Jr.; Ed.; American Chemical Society: Washington, D. C., 1988, and references therein. (g) LeGall, J.; Prickril, B. C.; Moura, I.; Xavier, A. V.; Moura, J. J. G.; Huynh, B.-H. *Biochemistry* **1988**, *27*, 1636-1642.

(3) (a) La Mar, G. N.; Eaton, G. R.; Holm, R. H.; Walker, F. A. *J. Am. Chem. Soc.* **1973**, *95*, 63-75. (b) La Mar, G. N.; Walker, F. N. *J. Am. Chem. Soc.* **1973**, *95*, 6950-6956. (c) Satterlee, J. D.; La Mar, G. N. *J. Am. Chem. Soc.* **1976**, *98*, 2804-2808. (d) Goff, H. M.; La Mar, G. N. *J. Am. Chem. Soc.* **1977**, *99*, 6599-6606. (e) Thanabal, V.; de Ropp, J. S.; La Mar, G. N. *J. Am. Chem. Soc.* **1988**, *110*, 3027-3035.

(4) (a) Lauffer, R. B.; Antanaitis, B. C.; Aisen, P.; Que, L., Jr. *J. Biol. Chem.* **1983**, *258*, 14212-14218. (b) Scarrow, R. C.; Pyrz, J. W.; Que, L., Jr. *J. Am. Chem. Soc.*, submitted.

(5) (a) Maroney, M. J.; Kurtz, D. M., Jr.; Nocek, J. M.; Pearce, L. L.; Que, L., Jr. *J. Am. Chem. Soc.* **1986**, *108*, 6871-6879. (b) Maroney, M. J.; Lauffer, R. B.; Que, L., Jr.; Kurtz, D. M., Jr. *J. Am. Chem. Soc.* **1984**, *106*, 6445-6446.

(6) Abbreviations used: *N*-MeIm, 1-methylimidazole; *N*-BuIm, 1-(*n*-butyl)imidazole; *N*-EtIm, 1-ethylimidazole; 5-MeIm, 5-methylimidazole; HIm, imidazole; py, pyridine; py-d_5, pyridine-d_5; TICOH, tris(*N*-methylimidazol-2-yl)hydroxymethane; TICO, monoanion of TICOH; TICOMe, 1,1,1-tris(*N*-methylimidazol-2-yl)methyl methyl ether; TIP, tris(imidazol-2-yl)phosphine; TMIP, tris(*N*-methylimidazol-2-yl)phosphine; O_2CMe, acetate; O_2CEt, propionate; O_2CBu^t, pivalate; O_2CPh, benzoate; salen, *N*,*N*′-ethylenebis(salicylideneamine); salhis, 4-[2′-(salicylideneamino)ethyl]imidazole; $HB(pz)_3$, tri-1-pyrazolylborate monoanion; hxta, 2-hydroxy-5-methyl-1,3-xylylenediamine-*N*,*N*,*N*′,*N*′-tetraacetate.

0002-7863/89/1511-6563$01.50/0 © 1989 American Chemical Society

complexes have been reported.[7,8] We have examined a set of ferric and ferrous imidazole complexes and a new set of binuclear and trinuclear iron clusters with the ligands and cluster types shown in Chart I. These complexes should provide an overview of the ^{1}H NMR behavior expected for imidazole ligands to paramagnetic non-heme iron in various oxidation and spin states and cluster types. With the exceptions of $[Fe(TICOH)_2]^{3+}$ and $[Fe(TICOMe)_2]^{3+}$,[7] ^{1}H NMR spectra of the complexes listed in Table I have not been reported previously, and no detailed analyses of the isotropic shifts have been reported for any of the complexes.

Experimental Section

Materials and Methods. Preparations of Compounds. Solvents and reagents (including deuterated compounds) were obtained mainly from Aldrich Chemical Co. and used without further purification unless otherwise noted. Hexanes, acetonitrile, and methylene chloride were distilled from CaH_2. Ethyl ether was distilled from sodium/benzophenone. N-MeIm and N-BuIm were vacuum distilled and stored over KOH pellets. N-MeIm-*d*, deuterated at the 2 position, was obtained by heating a mixture of N-MeIm and D_2O (1:4 v/v) at 50 °C for 2 days. $(Et_4N)_2[Fe_2OCl_6]$,[9] $(Et_4N)FeCl_4$,[10] $(Et_4N)_2FeCl_4$,[10] $TICOH\cdot{}^1/_2C_6H_6$,[11] TICOMe,[7] and $Na_2[Fe(CN)_5L]\cdot xH_2O$ (L = imidazoles[12]), TIP,[13] and TMIP[13] were prepared by previously described procedures. Syntheses and characterizations of $[Fe(TIP)_2](ClO_4)_3$, $[Fe(TMIP)_2](ClO_4)_3$, and the hemerythrin diiron(III) site models $[Fe_2O(O_2CMe)_2(TIP)_2](ClO_4)_2$, $[Fe_2O(O_2CR)_2(TMIP)_2]X_2$ (R = Me, Et, Ph; X = ClO_4; PF_6), $[Fe_2(OH)(O_2CMe)_2(TMIP)_2](ClO_4)_2BF_4$, and $[Fe_2(OH)(O_2CEt)_2(TMIP)_2](ClO_4)_3$ will be reported elsewhere.[14]

Warning! A small amount of solid $[Fe(TIP)_2](ClO_4)_3$ detonated violently while being scraped from a glass frit. We strongly recommend against preparation of perchlorate salts containing either TIP or TMIP.

Solvents used to prepare $[FeL_6]^{2+}$ and $[Fe_3O(O_2CR)_6L_3]$ (L = imidazoles) were thoroughly degassed by bubbling O_2-free N_2 or Ar through for at least 20 min. Schlenk-type glassware and vacuum-line manipulations were normally used. Elemental analyses were performed by Atlantic Microlabs, Inc., Atlanta, GA.

$[Fe(N\text{-EtIm})_6](BF_4)_2$. Reaction of $[Fe(CH_3CN)_6](BF_4)_2$[15] with ~10-fold molar excess of *N*-EtIm in methylene chloride led to formation of the product as a white solid. Unexceptional workup gave a 74% yield. Anal. Calcd for $C_{30}H_{48}N_{12}B_2F_8Fe$: C, 44.70; H, 5.96; N, 20.86. Found: C, 44.52; H, 5.99; N, 20.71.

$[Fe(N\text{-MeIm})_6](BPh_4)_2$ and $[Fe(5\text{-MeIm})_6](BPh_4)_2$. The procedure has been briefly described for $[Fe(N\text{-MeIm})_6](BPh_4)_2$.[16] An exemplary procedure is described here for preparation of $[Fe(5\text{-MeIm})_6](BPh_4)_2$. Absolute ethanol (110 mL) was added via cannula to a flask containing 1.92 g (9.66 mmol) of $FeCl_2\cdot4H_2O$ and 9.52 g (12 equiv) of 5-MeIm, and the mixture was stirred for 3 h. To the resulting light yellow-orange solution was added solid $NaBPh_4$ under Ar. After 15 min of stirring, NaCl was removed by filtration. Precipitation of the crude product was induced by removal of ~20 mL of solvent in vacuo. The white solid thus formed was collected by filtration and washed with anhydrous ethyl ether (30 mL × 2). Purification of this crude product was effected by dissolution of the solid in 60 mL of methylene chloride and reprecipitation by addition of ~100 mL of ethyl ether. This procedure resulted in formation of a layer of yellow oil on the bottom of the flask. The white suspension above this layer was transferred to another flask via cannula, and the solvent was removed in vacuo. The product (4.0 g, 35% yield) was obtained as a snow-white powder. Anal. Calcd for $C_{72}H_{76}N_{12}B_2Fe$: C, 72.85; H, 6.40; N, 14.15. Found: C, 73.03; H, 6.49; N, 14.03.

$[Fe_3O(O_2CR)_6L_3]X$, R = Me, Et, Bu^t, Ph; L = HIm, *N*-MeIm, *N*-BuIm, 5-MeIm; X = Cl, BF_4, BPh_4. A general approach, applicable to all of the combinations of carboxylates, imidazoles, and counteranions is exemplified by the procedure for preparation of $[Fe_3O(O_2CPh)_6(5\text{-MeIm})_3]BPh_4$. All manipulations were performed anaerobically to minimize moisture. To a solution prepared by 10 min of stirring of 0.80 g (1.33 mmol) of $(Et_4N)_2[Fe_2OCl_6]$ and 0.44 g (1 equiv) of $(Et_4N)FeCl_4$ in 20 mL of acetonitrile was added solid sodium benzoate (1.15 g, 6 equiv), and the solution was then vigorously stirred for 20 min. To the resulting deep orange-red suspension was added dropwise a solution of 4-methylimidazole (0.77 g, 7 equiv) in 20 mL of acetonitrile over 50 min. A large quantity of green solid formed when addition was complete. (When *N*-MeIm was used, the mixture remained homogeneous at this point; some acetonitrile was removed in vacuo, and ethyl ether added to force precipitation in this case.) After 2 h of stirring, the suspension was filtered, and the resulting green solid was treated with 0.46 g (1 equiv) of $NaBPh_4$ in 60 mL of methylene chloride. NaCl was removed by filtration, and the deep greenish-brown filtrate was carefully layered with 40 mL of hexanes. Deep-brown crystalline blocks were obtained after overnight diffusion. The mother liquor was transferred to another flask and cooled to −20 °C, which yielded additional product. The total yield after pumping to dryness was 1.28 g (65%). The compound can be recrystallized from hexanes/dichloromethane. Anal. Calcd for $C_{24}H_{68}N_6BFe_3O_{13}$: C, 63.48; H, 4.64; N, 5.69. Found: C, 63.33; H, 4.69; N, 5.76. **$[Fe_3O(O_2CMe)_6(N\text{-MeIm})_3]BPh_4\cdot CH_2Cl_2$.** The yield was 45%. Anal. Calcd for $C_{49}H_{58}N_6BCl_2Fe_3O_{13}$: C, 49.53; H, 4.92; N, 7.11. Found: C, 49.66; H, 4.91; N, 7.06. Room-temperature effective magnetic moment in acetonitrile: 3.34 μ_B/Fe. **$[Fe_3O(O_2CPh)_6(N\text{-BuIm})_3]BF_4$.** The yield was 68%. Anal. Calcd for $C_{63}H_{66}N_6BF_4Fe_3O_{13}$: C, 55.25; H, 4.86; N, 6.14. Found: C, 55.51; H, 4.88; N, 6.19. Room-temperature effective magnetic moment in acetonitrile: 3.40 μ_B/Fe. **$[Fe_3O(O_2CEt)_6(5\text{-MeIm})_3]Cl$.** Due to the high solubility of this compound in acetonitrile, separation from Et_4NCl and other side products presented a problem. The compound was isolated as green needles in 5% yield by cooling the reaction mixture in acetonitrile at −20 °C overnight. Anal. Calcd for $C_{30}H_{48}N_6Cl_2Fe_3O_{13}$: C, 39.87; H, 5.35; N, 9.30. Found: C, 39.81; H, 5.24; N, 9.14.

$[Fe_3O(O_2CR)_6L_3]$ R = Me, Ph; L = HIm, 1-MeIm, 5-MeIm. These mixed-valent complexes can be prepared either by ligand replacement on $[Fe_3O(O_2CR)_6(H_2O)_3]$[17] by imidazoles according to a previously described procedure for the analogous pyridine complexes[17,18] or by reactions using $(Et_4N)_2[Fe_2OCl_6]$ and $(Et_4N)_2FeCl_4$ as starting materials. The latter approach is exemplified by the preparation of **$[Fe_3O(O_2CPh)_6(5\text{-MeIm})_3]\cdot Et_4NCl$.** A solution of 0.88 g (1.33 mmol) of $(Et_4N)_2[Fe_2OCl_6]$ and 0.63 g (1 equiv) of $(Et_4N)_2FeCl_4$ in 30 mL of acetonitrile was stirred for 30 min; solid sodium benzoate (1.15 g, 6 equiv) was then added with vigorous stirring. The resulting deep-orange suspension was stirred for 90 min. Then a solution of 0.66 g (6 equiv) of 4-methylimidazole in 20 mL of acetonitrile was added dropwise over the course of 40 min. Upon complete addition, a black solution formed that contained undissolved NaCl. The mixture was stirred for an additional 2 h and then filtered to remove NaCl. A green suspension was obtained by concentrating the filtrate to ~35 mL and adding ~40 mL of ethyl ether. After collection by filtration, the resulting green solid was recrystallized from ethyl ether/acetonitrile in the presence of a small amount of excess 4-methylimidazole. The product (0.86 g, 55%) was obtained as small black plates. Anal. Calcd for $C_{62}H_{68}N_7ClFe_3O_{13}$: C, 56.33; H, 5.18; N, 7.35. Found: C, 56.33; H, 5.25; N, 7.50. The presence of Et_4NCl was indicated by both elemental analysis and ^{1}H NMR. **$[Fe_3O(O_2CMe)_6(N\text{-MeIm})_3]$.** This complex was prepared via ligand substitution on $[Fe_3O(O_2CR)_6(H_2O)_3]$. The yield was 74%. Anal. Calcd for $C_{24}H_{36}N_6Fe_3O_{13}$: C, 36.76; H, 4.63; N, 10.72. Found: C, 36.67; H, 4.49; N, 10.60. Room-temperature effective magnetic moment in acetonitrile: 3.09 μ_B/Fe. **$[Fe_3O(O_2CPh)_6(N\text{-MeIm})_3]$.** This complex was prepared by using $(Et_4N)_2[Fe_2OCl_6]$ and $(Et_4N)_2FeCl_4$ as described above. The yield was 68%. Anal. Calcd for $C_{54}H_{48}N_6Fe_3O_{13}$: C, 56.08; H, 4.18; N, 7.27. Found: C, 55.35; H, 4.22; N, 7.05.

$[Fe_2MgO(O_2CR)_6L_3]$, R = Me, Ph; L = HIm, *N*-MeIm, 5-MeIm, py-d_5. The acetate-bridged complexes were prepared by ligand substitution on $[Fe_2MgO(O_2CMe)_6(H_2O)_3]$ with neat *N*-MeIm or py-d_5.[19] **$[Fe_2MgO(O_2CMe)_6(N\text{-MeIm})_3]\cdot{}^3/_4CH_2Cl_2$.** The yield was 72%. The presence of CH_2Cl_2 was indicated by ^{1}H NMR. Anal. Calcd for $C_{24.75}H_{37.5}N_6Cl_{1.5}Fe_2MgO_{13}$: C, 36.43; H, 4.63; N, 10.30. Found: C, 36.55; H, 4.58; N, 10.28. Effective magnetic moment at 297 K in ace-

(7) Gorun, S. M. Ph.D. Thesis, 1986, Massachusetts Institute of Technology, Cambridge, MA.
(8) Tao, X.; Stephan, D. W.; Mascharack, P. K. *Inorg. Chem.* **1987**, *26*, 754–759.
(9) Armstrong, W. H.; Lippard, S. J. *Inorg. Chem.* **1985**, *24*, 981–982.
(10) Gill, N. S.; Taylor, F. B. *Inorg. Synth.* **1967**, *9*, 136–142.
(11) Tang, C. C.; Davalian, D.; Huang, P.; Breslow, R. *J. Am. Chem. Soc.* **1978**, *100*, 3918–3922.
(12) Johnson, C. R.; Sheperd, R. E.; Marr, B.; O'Donnel, S.; Dressick, W. *J. Am. Chem. Soc.* **1980**, *102*, 6227–6235.
(13) Curtis, N. J.; Brown, R. S. *J. Org. Chem.* **1980**, *45*, 4038–4040.
(14) Wu, F.-J.; Kurtz, D. M., Jr.; Debrunner, P. G.; Nyman, P., manuscript in preparation.
(15) Hathaway, B. J.; Holah, D. G.; Underhill, A. E. *J. Chem. Soc.* **1962**, 2444–2448.
(16) Miller, L. L.; Jacobson, R. A.; Chen, Y.-S.; Kurtz, D. M., Jr. *Acta Crystallogr., Sect. C* **1989**, *C45*, 527–529.
(17) (a) Oh, S. M.; Hendrickson, D. N., Hassett, K. L.; Davis, R. E. *J. Am. Chem. Soc.* **1985**, *107*, 8009–8018. (b) Dziobkowski, C. T.; Wrobleski, J. T.; Brown, D. B. *Inorg. Chem.* **1981**, *20*, 679–684.
(18) Lupu, D.; Ripan, R. *Rev. Roum. Chim.* **1971**, *16*, 43–44.
(19) (a) Blake, A. B.; Yavari, A.; Hatfield, W. E.; Sethulekshmi, C. N. *J. Chem. Soc., Dalton Trans.* **1985**, 2509–2520. (b) Blake, A. B.; Yavari, A.; Kubicki, H. *J. Chem. Soc., Chem. Commun.* **1981**, 796–797.

tonitrile: 2.38 μ_B/Fe (very close to the solid-state value reported for the pyridine congener).[19] This same complex containing a perdeuterated acetate methyl group was prepared via ligand substitution on $[Fe_2MgO(O_2CMe\text{-}d_3)_6(H_2O)_3]$. The benzoate-bridged complexes were prepared by using $(Et_4N)_2[Fe_2OCl_6]$ and $MgCl_2$. This latter procedure is described for $[Fe_2MgO(O_2CPh)_6(5\text{-MeIm})_3]\cdot{}^4/_3Et_4NCl$. A suspension of 0.80 g (1.33 mmol) of $(Et_4N)_2[Fe_2OCl_6]$ and 0.14 g (1.47 mmol) in 20 mL of acetonitrile was stirred for 50 min; 1.15 g (6 equiv) of solid sodium benzoate was then added. After vigorous stirring of the resulting orange-brown suspension for 50 min, 0.66 g (6 equiv) of 4-methylimidazole in 20 mL of acetonitrile was added dropwise over the course of 1 h. A green suspension formed when addition was complete; the mixture was stirred for an additional 2 h. After addition of 50 mL of ethyl ether, a green precipitate was collected by filtration and pumped to dryness in vacuo. The green solid was redissolved in 50 mL of acetonitrile and filtered to remove NaCl. The green filtrate was diluted with 30 mL of acetonitrile and then layered with 10 mL of hexanes and 60 mL of ether. Deep-brown plates (0.81 g, 45%) of $[Fe_2MgO(O_2CPh)_6(5\text{-MeIm})_3]\cdot{}^4/_3Et_4NCl$ appeared when diffusion was complete. The presence of Et_4NCl was indicated by both ^1H NMR and elemental analysis. Anal. Calcd for $C_{64.7}H_{74.7}N_{7.33}Cl_{1.33}Fe_3MgO_{13}$: C, 57.72; H, 5.59; N, 7.63; Cl, 3.52. Found: C, 57.50; H, 5.43; N, 7.54; Cl, 3.53.

$[Fe(TICOH)_2]X_3$, X = Cl, BF_4; $[Fe(TICOMe)_2](ClO_4)_3$. To a solution of 0.13 g (0.80 mmol) $FeCl_3$ in 30 mL of acetonitrile was added 0.51 g (1.62 mmol) of $TICOH\cdot{}^1/_2C_6H_6$. The resulting mixture was stirred for 3 h. The brown precipitate thus formed was collected by filtration. The filtrate was cooled to −20 °C to yield additional product as black crystals. After being pumped to dryness in vacuo, the solid $[Fe(TICOH)_2]Cl_3$ weighed 0.46 g (95% yield). Metathesis with $NaBF_4$ in acetonitrile gave $[Fe(TICOH)_2]BF_4$ in essentially quantitative yield. Room-temperature effective magnetic moment in acetonitrile: 2.70 μ_B/Fe. $[Fe(TICOMe)_2](ClO_4)_3$ was prepared by a similar procedure in >90% yield in acetonitrile. The ^1H NMR spectra of these complexes in CD_3CN were essentially identical with those reported in ref 7.

Physical Measurements. ^1H NMR spectra were recorded at 300 K (unless otherwise noted) with either Bruker AM250 or AM500 spectrometers operating at ^1H frequencies of 250 and 500 MHz, respectively. The signal-to-noise ratio was improved by introducing 2–15 Hz of line broadening, the exact magnitude of which depended on the sweep width. Chemical shifts were referenced to $(CH_3)_4Si$ at 300 K. Downfield and upfield shifts are reported as positive and negative, respectively. Values reported in Tables I and III are *observed* chemical shifts. Isotropic shifts of imidazole ligand protons (methyls) were calculated from the observed shifts by subtraction of the following diamagnetic shifts of imidazoles in ppm: N(1)-H, 8.5 (3.4); 2-H, 7.2; 4-H, 7.0; 5-H, 7.0 (2.2). These "free-ligand" shifts were considered to be sufficiently accurate for our purposes, since the low-spin, diamagnetic ferrous complex $[Fe(CN)_5(N\text{-MeIm})]^{3-}$ is reported to have imidazole ring proton and methyl shifts within 0.2 ppm of those for the free ligand.[20] The following additional diamagnetic shifts (in ppm) were used for TICOH and TICOMe, respectively: OH, 6.75; OCH_3, 3.51. ^1H spin–lattice relaxation times, T_1, were measured by using the conventional 180°–τ–90° method.[21] Solution magnetic moments were measured in CD_3CN by the modified Evans method with $(CH_3)_4Si$ as the reference.[22] Diamagnetic corrections were calculated by using published values for the various substituents.[23] The value for pyridine was used to approximate that of imidazole.

Results and Discussion

We first summarize the relevant, general considerations that can be used to analyze ^1H NMR spectra of paramagnetic ferric and ferrous complexes.[2c,24,25] The isotropic shift (i.e., the observed chemical shift minus a reference diamagnetic shift) is the sum of contact and dipolar contributions:

$$(\Delta H/H)^{iso} = (\Delta H/H)^{con} + (\Delta H/H)^{dip} \quad (1)$$

The proportion of these two contributions depends on the oxidation and spin state of iron. The singlet oribtal ground state of high-spin Fe(III) normally results in only contact contributions to the isotropic shift. This ground state also results in a relatively long electron spin–lattice relaxation time, T_{1e}, which tends to broaden the ligand NMR resonances according to $T_1^{-1} \propto T_{1e}r^{-6}$, where T_1 is the ^1H spin–lattice relaxation time and r is the length of the Fe–H distance vector. For long T_{1e}'s such as in high-spin Fe(III), rotational correlation times can also affect T_1^{-1}. The triplet orbital ground states of octahedral low-spin Fe(III) and high-spin Fe(II) generally give rise to both contact and dipolar contributions to isotropic shifts and also to shorter T_{1e}'s, which result in narrower resonances than for high-spin Fe(III). For all three cases the ^1H T_1 is proportional to r^{-6}, which means that T_1 measurements can assist in assigning resonances. (Ligand-centered dipolar effects can sometimes modulate this dependence in conjugated systems.) For ligands in paramagnetic ferric and ferrous complexes, the proton T_1 and T_2 (the spin–spin relaxation time) are essentially equal, meaning that the proton T_1 is reflected in the linewidth. In this work we have assigned resonances by a combination of T_1 measurements, atom substitution, and integrated area ratios. The contact and dipolar contributions usually show T^{-1} and T^{-2} temperature dependences, respectively, which can sometimes be used to separate these contributions. The imidazole ligand numbering system used in the following discussion is shown in I.

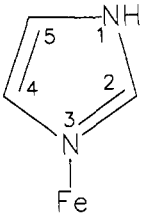

I

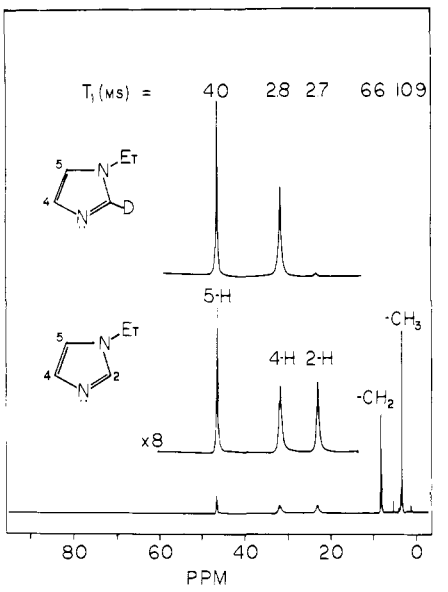

Figure 1. ^1H NMR spectra of $[Fe(N\text{-EtIm})_6](BF_4)_2$ in CD_2Cl_2 at 300 K. ^1H T_1 values in milliseconds are listed above each resonance.

High-Spin Fe(II). Previous measurements of effective magnetic moments and Mössbauer isomer shifts indicate that ferrous hexakis(imidazole) complexes are high-spin at 300 K.[26a] A change to 4-coordination in solution is unlikely for $[Fe(N\text{-RIm})_6]^{2+}$ and $[Fe(5\text{-MeIm})_6]^{2+}$; this stoichiometry has been observed only for the sterically hindered complexes with 2-MeIm and 1,2-Me_2Im.[26b,c] ^1H NMR data for $[Fe(N\text{-EtIm})_6]^{2+}$ are shown in Figures 1 and 2. Table I lists chemical shifts for $[Fe(N\text{-MeIm})_6]^{2+}$, $[Fe(N\text{-}$

(20) Johnson, C. R.; Henderson, W. W.; Sheperd, R. E. *Inorg. Chem.* **1984**, *23*, 2754–2763.
(21) Vold, R. L.; Waugh, J. S.; Klein, M. P.; Phelps, D. E. *J. Am. Chem. Phys.* **1968**, *48*, 3831–3832.
(22) Bailey, R. A. *J. Chem. Educ.* **1972**, *49*, 297–299.
(23) Angelici, R. J. *Synthesis and Technique in Inorganic Chemistry*, 2nd ed.; W. B. Saunders: Philadelphia, PA, 1977; p 49.
(24) Bertini, I.; Luchinat, C. *NMR of Paramagnetic Molecules in Biological Systems*; Benjamin/Cummings: Menlo Park, CA, 1986.
(25) (a) Horrocks, W. DeW, Jr. In *NMR of Paramagnetic Molecules*; La Mar, G. N., Horrocks, W. deW., Jr., Holm, R. H., Eds.; Academic Press: New York, 1973; pp 127–177. (b) La Mar, G. N. *Ibid.*, pp 85–126.

(26) (a) Reedijk, J. *Recl. Trav. Chim. Pays-Bas* **1971**, *90*, 1285–1291. (b) Reedijk, J. *Recl. Trav. Chim. Pays-Bas* **1972**, *91*, 507–516. (c) *Ibid.* 1373–1382.

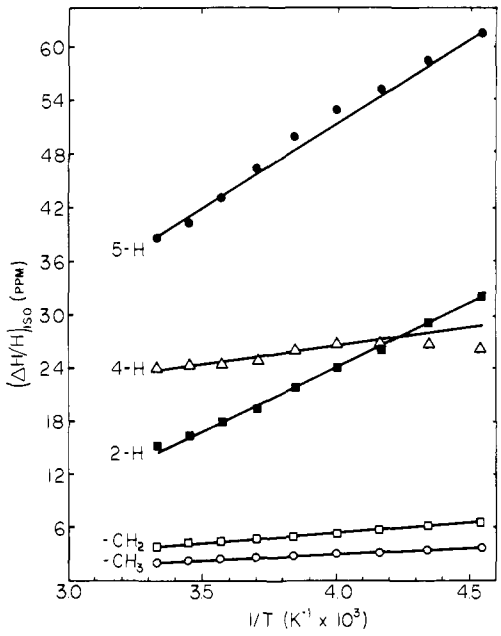

Figure 2. Temperature dependence of imidazole ^1H NMR isotropic shifts of $[Fe(N\text{-}EtIm)_6](BF_4)_2$ in CD_2Cl_2.

$EtIm)_6]^{2+}$, and $[Fe(5\text{-}MeIm)_6]^{2+}$. Ligand resonances were assigned by a combination of T_1 measurements and atom substitution, as exemplified in Figure 1. All ligand H and CH_3 resonances are shifted downfield from their diamagnetic positions at 300 K. With the exception of the 4-H resonance, all ligand resonances show Curie temperature dependences. In contrast to a previous study of the ^1H NMR spectrum of $[Fe(HIm)_6]^{2+}$ in CD_3OD,[27] use of $[Fe(N\text{-}RIm)_6]^{2+}$ in the relatively noncoordinating solvent, CD_2Cl_2, allows us to resolve 4-H and 5-H resonances of coordinated imidazole. The relative T_1 values at 300 K and the linear temperature dependences argue against ligand-exchange effects on the spectrum of $[Fe(N\text{-}RIm)_6]^{2+}$. Exchange broadening is evident in spectra of $[Fe(5\text{-}MeIm)_6]^{2+}$ at 300 K, especially for the N–H resonance. The minor effects of this exchange on the observed shifts can be gauged from comparison with the 300 K shifts obtained from linear extrapolations of the $1/T$ plots (listed in parentheses in Table I). In the cases of effectively octahedral $[Fe(N\text{-}EtIm)_6]^{2+}$ and $[Fe(5\text{-}MeIm)_6]^{2+}$, dipolar contributions to the isotropic shifts are expected to be negligible.[25,27] Direct σ spin delocalization was proposed to be the predominant mechanism contributing to contact shifts of the imidazole ligand protons in ferrous heme complexes.[3d] This mechanism results in downfield isotropic shifts for all ligand H's, but the shifts do *not* decrease monotonically with increasing number of bonds from the metal atom. The same pattern is observed for the hexakis(imidazole) complexes where the order of chemical shifts at 300 K is N(1)-H > 5-H > 4-H > 2-H > N-CH_3 > 5-CH_3. The anti-Curie behavior of the 4-H resonance at low temperature suggests that rotational restrictions of the imidazole ring around the Fe–N bond may come into play. Freezing out of a structure having less than O_h symmetry (e.g., D_{3d}) with the 4-H equatorial to the principal magnetic axis would induce upfield dipolar contributions to the isotropic shifts. Such dipolar contributions are explicitly analyzed in the next section.

Low-Spin Fe(III). The line widths of the ligand imidazole resonances in the low-spin ferric complexes (Table I and Figures 3 and 4) are all significantly narrower than those of the high-spin ferric complexes, reflecting the relatively shorter T_{1e} of low-spin Fe(III). Primarily for this reason the imidazole ligand 2-H and 4-H resonances are readily observed in spectra of these low-spin ferric complexes. The crystal structure of $[Fe(TICOH)_2]^{3+}$[7] shows an FeN_6 coordination sphere with ligation through imidazole N-3.

(27) Wicholas, M.; Mustacich, R.; Johnson, B.; Smedley, T.; May, J. *J. Am. Chem. Soc.* **1975**, *97*, 2113–2115.

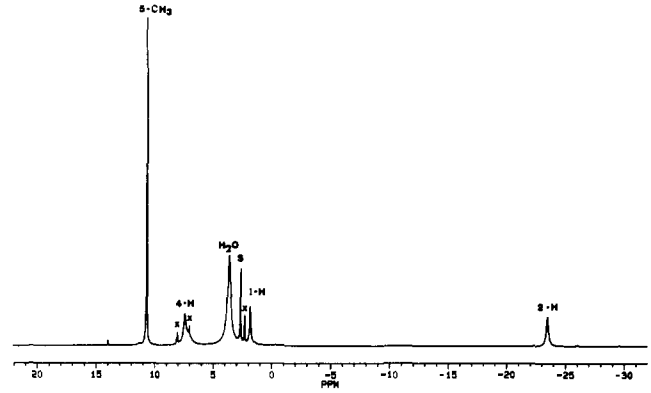

Figure 3. ^1H NMR spectra of $Na_2[Fe(CN)_5(5\text{-}MeIm)]\cdot xH_2O$ in DMSO-d_6 at 300 K. S denotes solvent resonance; × denotes free imidazole resonances.

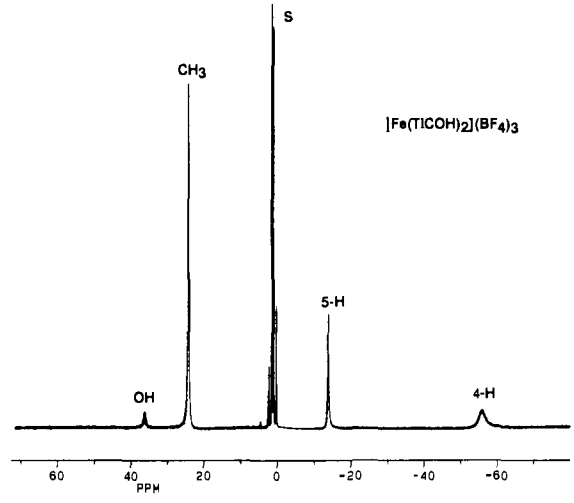

Figure 4. ^1H NMR spectra in CD_3CN at 300 K of $[Fe(TICOH)_2](BF_4)_3$. S = solvent.

T_1 values of 0.66 and 4.63 ms were used to assign the imidazole ligand 4-H and 5-H resonances, respectively, of $[Fe(TICOH)_2]^{3+}$ and by analogy of $[Fe(TICOMe)_2]^{3+}$. The isotropic shifts in ppm calculated from the data for the ferric pentacyanoimidazole complexes listed in Table I are as follows: N(1)-H, −6.2; N-CH_3, 13.1; 2-H, −27.5; 4-H, −0.5; 5-H, −6.4; 5-CH_3, 8.3. The alternating signs of H and CH_3 isotropic shifts at both the N-1 and C-5 positions indicate that π spin delocalization is responsible for the contact contributions, as expected for the t_{2g}^5 d-electron configuration. For π spin delocalization, one expects exclusively upfield contact contributions for all imidazole ring protons and downfield contributions for all ring methyls.[3c] However, for low-spin ferric ion in an environment of less than cubic symmetry, dipolar contributions to the isotropic shifts must also be considered. These contributions can be analyzed according to the equation

$$(\Delta H/H)^{dip} = (1/3N)(\chi_{\parallel} - \chi_{\perp})(3\cos^2\theta - 1)r^{-3} \qquad (2)$$

where N is Avogadro's number, $\chi_{\parallel}$ and $\chi_{\perp}$ are the molar susceptibilities parallel and perpendicular to the unique magnetic axis, and θ is the angle between the Fe–H distance vector, r, and the unique magnetic axis.[3] The diagrams of Figure 5 show the assumed orientations of the imidazole ligands with respect to the principal magnetic axes for $[Fe(CN)_5(Im)]^{2-}$ and $[Fe(TICOH)_2]^{3+}$. According to eq 2, the assumed orientation of imidazole for $[Fe(CN)_5(Im)]^{2-}$ will result in exclusively downfield dipolar contributions to the isotropic shifts of all imidazole ring protons and methyls. A combination of upfield (or downfield for methyls) contact and downfield dipolar contributions is qualitatively consistent with the isotropic shifts listed above for the ferric pentacyanoimidazole complexes. For these complexes the imidazole 2-H was assigned by deuterium labeling to a resonance that

Table I. ^1H NMR Chemical Shifts at 300 K in Non-Heme Iron Imidazole Complexes and Clusters

complex[a]	chemical shifts, ppm: imidazole ligand N(1)-H or N(1)-R	2-H	4-H	5-H or 5-Me	RCO_2^-	other
high-spin Fe(II)						
$[Fe(N\text{-MeIm})_6](BPh_4)_2$[b]	8.9 Me	26.4	29.0	46.9		
$[Fe(N\text{-EtIm})_6](BF_4)_2$[b]	8.1, 3.4 Et	23.1	31.9	46.7		
$[Fe(5\text{-MeIm})_6](BPh_4)_2$[b,h]	64.5 (69.5)	26.9 (27.9)	28.7 (28.7)	6.8 Me (6.9)		
low-spin Fe(III)						
$[Fe(TICOH)_2](BF_4)_3$[c]	25.1 Me		−54.8	−12.9		37.1 OH
$[Fe(TICOH)_2]Cl_3$[d]	24.8 Me		−53.2	−12.1		n.o.[g] OH
$[Fe(TICOMe)_2](ClO_4)_3$[c]	24.6 Me		−54.1	−11.7		21.6 OMe
$[Fe(TMIP)_2](ClO_4)_3$[c]	23.8 Me		−53.4	−11.0		
$[Fe(TIP)_2](ClO_4)_3$[c,i]	9.1		−50.9	−9.4		
$Na_2[Fe(CN)_5(N\text{-MeIm})]\cdot xH_2O$[e]	16.6 Me	−17.2	7.2	0.4		
$Na_2[Fe(CN)_5(5\text{-MeIm})]\cdot xH_2O$[e]	1.7	−23.6	7.3	10.5 Me		
$Na_2[Fe(CN)_5(HIm)]\cdot xH_2O$[e]	2.9	−19.1	5.1	0.9		
high-spin Fe(III)						
$[Fe_2O(O_2CMe)_2(TMIP)_2](ClO_4)_2$[c]	5.1, 4.6 Me		n.o.	13.9, 11.3	10.1 Me	
$[Fe_2O(O_2CMe)_2(TIP_2)](ClO_4)_2$[c]	19.2, 15.1		n.o.	13.4, 10.9	10.2 Me	
$[Fe_2O(O_2CEt)_2(TMIP)_2](PF_6)_2$[c]	5.1, 4.5 Me		n.o.	13.9, 11.2	9.3, 2.8 Et	
$[Fe_2O(O_2CPh)_2(TMIP)_2](PF_6)_2$[c]	5.3, 4.7 Me		n.o.	14.0, 11.4	8.7*m*, 8.0*o*, 7.0*p*	
$[Fe_2(OH)(O_2CMe)_2(TMIP)_2](ClO_4)_2BF_4$[c]	17.1, 16.0 Me		n.o.	60.6	65.9 Me	
$[Fe_2(OH)(O_2CEt)_2(TMIP)_2](ClO_4)_3$[c]	16.8, 15.6 Me		n.o.	59.4	~57.0, 14.0 Et	
$[Fe_2MgO(O_2CMe\text{-}d_3)_6(N\text{-MeIm})_3]$[b]	4.5 Me	n.o.	n.o.	13.7		
$[Fe_2MgO(O_2CPh)_6(N\text{-MeIm})_3]$[c]	4.8 Me	n.o.	n.o.	14.4	9.7, 7.1, 8.6, 6.8 Ph	
$[Fe_2MgO(O_2CPh)_6(5\text{-MeIm})_3]$[c]	20.5	n.o.	n.o.	4.0 Me	9.7, 7.0, 8.6, 6.8 Ph	
$[Fe_2MgO(O_2CPh)_6(HIm)_3]$[c]	20.6	n.o.	n.o.	14.2	9.7, 7.0, 8.6, 6.8 Ph	
$[Fe_3O(O_2CMe)_6(N\text{-MeIm})_3]BPh_4$[b]	8.4 Me	21.9	34.3	27.1	30.7 Me	
$[Fe_3O(O_2CEt)_6(N\text{-MeIm})_3]BPh_4$[b]	8.2 Me	21.7	34.1	26.7	25.1, 7.6 Et	
$[Fe_3O(O_2CBu^t)_6(HIm)_3]BPh_4$[f]	34.7	22.2	32.1	26.3	8.1 Bu^t	
$[Fe_3O(O_2CBu^t)_6(5\text{-MeIm})_3]BPh_4$[c]	32.9	22.8	31.4	7.7 Me	8.1 Bu^t	
$[Fe_3O(O_2CPh)_6(N\text{-BuIm})_3]BF_4$[b]	8.4, 3.0, 1.8, 1.2 Bu	22.8	34.7	27.9	12.0*m*, 8.4*o*, 5.4*p* Ph	
$[Fe_3O(O_2CPh)_6(HIm)_3]BF_4$[c]	35.3	22.7	33.4	27.5	12.0*m*, 8.2*o*, 5.3*p* Ph	
$[Fe_3O(O_2CPh)_6(5\text{-MeIm})_3]BPh_4$[c]	35.3	23.3	32.7	8.7 Me	12.1*m*, 8.3*o*, 5.3*p* Ph	
high-spin, mixed-valence						
$[Fe_3O(O_2CMe)_6(N\text{-MeIm})_3]$[b]	4.6 Me	12.2	19.7	17.9	15.7 Me	
$[Fe_3O(O_2CPh)_6(N\text{-MeIm})_3]$[b]	4.9 Me	13.7	22.0	18.4	10.1*m*, 10.5*o*, 7.8*p* Ph	
$[Fe_3O(O_2CPh)_6(5\text{-MeIm})_3]$[c]	25.4	13.8	19.5	3.5 Me	10.2*m*, 10.6*o*, 7.9*p* Ph	

[a-f] Solvents are [b] CD_2Cl_2, [c] CD_3CN, [d] CD_3OD, [e] DMSO-d_6, [f] acetone-d_6. [g] Not observed. [h] Values in parentheses are extrapolated from linear portion of 1/T plot. [i] cf. **Warning** in Experimental Section.

appears much farther upfield than that assigned to the 4-H. The observed 2-H and 4-H shifts are consistent with the much larger upfield contact contributions to the 2-H isotropic shifts obtained for low-spin ferric heme imidazole complexes.[3c]

The structure of $[Fe(TICOH)_2]^{3+}$ is known,[7] and, hence, the geometric factors for the constituent protons can be calculated in this case. A quantitative analysis also requires evaluation of the magnetic factor in eq 2. For this evaluation we adapt a method that has been used to separate the contact and dipolar contributions to the isotropic shifts of low-spin ferric tetraphenylporphyrin complexes.[3a,c] As discussed above, we assume that the imidazole contact shifts are due exclusively to π spin delocalization. If so, then the isotropic shifts of OH and OCH_3 in $[Fe(TICOH)_2]^{3+}$ and $[Fe(TICOMe)_2]^{3+}$, respectively, should be exclusively dipolar in origin, since these protons are separated by three and four σ bonds, respectively, from the π system of imidazole. Making the preceding assumptions in the case of $[Fe(TICOH)_2]^{3+}$, the dipolar shift for any remaining proton, *i*, in the cation can be calculated from the isotropic shift of the OH and the relative geometric factor:

$$(\Delta H/H)_i^{dip} = (\Delta H/H)_{OH}^{dip}\{(3\cos^2\theta - 1)r^{-3}\}_i/\{(3\cos^2\theta - 1)r^{-3}\}_{OH} \quad (3)$$

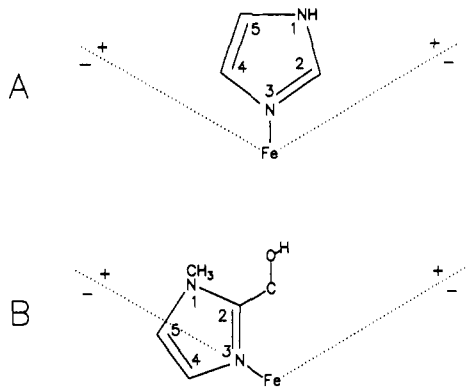

Figure 5. Schematic orientations of imidazole rings with respect to principal susceptibility axes centered on the iron atoms in (A) $[Fe(CN)_5(Im)]^{2-}$ and (B) $[Fe(TICOH)_2]^{3+}$. The axis of $\chi_\parallel$ is oriented vertically. The dotted lines indicate cones of the magic angle around $\chi_\parallel$. The signs of dipolar contributions to the isotropic shifts of imidazole protons axial (+) and equatorial (−) to the cone for $0° < \theta < 90°$ are indicated, assuming $\chi_\parallel > \chi_\perp$.

Table II. Separation of ^1H NMR Isotropic Shifts of $[Fe(TICOH)_2]^{3+}$ into Contact and Dipolar Contributions[a]

position	$(\Delta H/H)^{iso}$	$10^{21}(3\cos^2\theta - 1)r^{-3}$ [b]	$(\Delta H/H)^{dip}$	$(\Delta H/H)^{con}$
N-CH_3	21.6 (21.2)	6.7 (6.7)	12.0 (10.8)	9.6 (10.4)
4-H	−61.8 −(61.1)	−31.7 (−31.7)	−56.7 (−51.2)	−5.1 (−9.9)
5-H	−19.9 (−18.7)	−2.9 (−2.9)	−5.2 (−4.7)	−14.7 (−14.0)
OH(OCH_3)	30.4 (18.1)	17.0 (11.2)[c]	30.4 (18.1)	0 (0)

[a] Calculated from observed shifts in ppm at 300 K in CH_3CN, by using eq 1–3 in the text. Values in parentheses are for $[Fe(TICOMe)_2]^{3+}$. [b] In units of cm^{-3}, calculated from atomic coordinates listed in ref 7 and with the assumption that $[Fe(TICOMe)_2]^{3+}$ is isostructural with $[Fe(TICOH)_2]^{3+}$. [c] For the ether linkage a C–O–C bond angle of 110.6° and a C–O bond distance of 1.39 Å were assumed; for the OCH_3 group a C–H distance of 1.0 Å was assumed.

The analogous equation can be written for OCH_3 in $[Fe(TICOMe)_2]^{3+}$. Table II summarizes the results of such calculations. The calculated dipolar and contact shifts have magnitudes and signs fully consistent with the preceding discussion. The very similar values obtained for $[Fe(TICOH)_2]^{3+}$ and $[Fe(TICOMe)_2]^{3+}$ further supports the validity of this analysis. The calculated contact contributions for $[Fe(TICOH)_2]^{3+}$ and $[Fe(TICOMe)_2]^{3+}$ have the same sign as and are within 7 ppm of those calculated for corresponding imidazole ring positions in low-spin ferric heme adducts.[3c] Differences of this magnitude in the two systems are reasonable; the porphyrin ring may affect the degree of π spin transfer to the axial imidazole. The chemical shifts observed for $[Fe(TICOH)_2]^{3+}$ and $[Fe(TICOMe)_2]^{3+}$ are very similar to those of $[Fe(TMIP)_2]^{3+}$, which indicates that different substituents at the 2 position of the imdiazol-2-yl group are without significant effect on the spin delocalization pathway(s).

High-Spin Fe(III). As with high-spin Fe(II), delocalization of unpaired spin primarily through the σ bond system of imidazole is expected, leading to downfield contact shifts for all ring protons and methyl groups. Generally, no dipolar contributions are expected, and the isotropic shifts should track the molar susceptibility per iron atom. For mononuclear complexes, the observed N(1)–H shift is ~100 ppm, and the 5-H ~80 ppm. The 2-H and 4-H are not observed due to their proximity to iron.[2c,4a] Since the preceding data are fairly well established for mononuclear complexes, we have examined clusters in the present work.

The dinuclear high-spin ferric imidazole complexes examined in this work are the new hemerythrin site models $[Fe_2O(O_2CMe)_2(TIP)_2]^{2+}$, $[Fe_2O(O_2CR)_2(TMIP)_2]^{2+}$, $[Fe_2(OH)(O_2CR)_2(TMIP)_2]^{3+}$, and $[Fe_2(OH)(O_2CR)_2(TMIP)_2]^{3+}$ (R = Me, Et, Ph) and the diiron-magnesium clusters $[Fe_2MgO(O_2CR)_6L_3]$ (L = imidazoles). The structures of these complexes are diagrammed schematically in Chart I. Analysis of the bridging acetate methyl resonances in these clusters is deferred to a later section. ^1H NMR spectra of the hemerythrin diiron site models

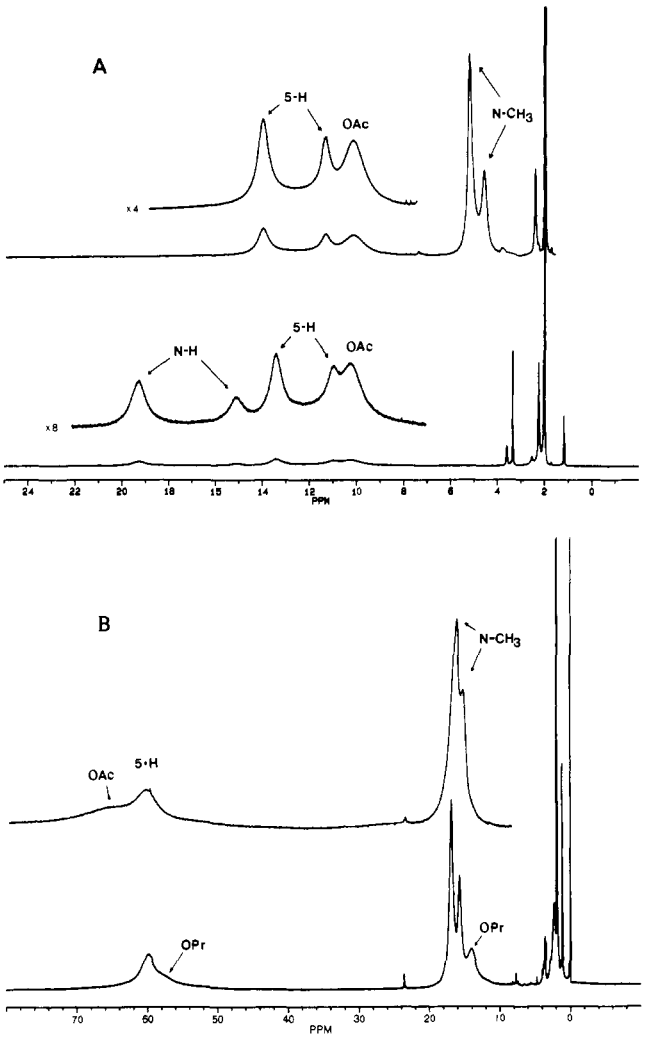

Figure 6. ^1H NMR at 300 K in CD_3CN of (A) $[Fe_2O(O_2CMe)_2(TMIP)_2](ClO_4)_2$ (upper) and $[Fe_2O(O_2CMe)_2(TIP)_2](ClO_4)_2$ (lower) and (B) $[Fe_2(OH)(O_2CMe)_2(TMIP)_2](ClO_4)_2BF_4$ (upper) and $[Fe_2(OH)(O_2CEt)_2(TMIP)_2](ClO_4)_3$ (lower).

are shown in Figure 6. As is the case for mononuclear complexes,[2c,4a] the imidazole ligand 4-H (and 2-H for the diiron–magnesium clusters) resonances are apparently broadened into the base line; the 5-H and N(1)-H are the only observable imidazole ring proton resonances in these binuclear high-spin ferric complexes. The structures of the hemerythrin models (Chart I) have imidazole ligands that are cis and trans to the μ-oxo bridge in a respective ratio of 2:1; we have assigned pairs of resonances in the spectra of $[Fe_2O(O_2CMe)_2(TIP)_2]^{2+}$ and $[Fe_2O(O_2CMe)_2(TMIP)_2]^{2+}$ to imidazole N(1)-H and N-CH_3, respectively, and to imidazole 5-H. Within each pair the lower field and higher field resonances are assigned to the cis and trans positions, respectively. These assignments are consistent with the expected trans effect of the μ-oxo bridge and with the area ratios within each pair (cf. Figure 6A). The imidazole 5-H and N-CH_3 resonances in spectra of the μ-hydroxo-bridged $[Fe_2(OH)(O_2CMe)_2(TMIP)_2]^{3+}$ and $[Fe_2(OH)(O_2CEt)_2(TMIP)_2]^{3+}$ (Figure 6B) are less well-resolved, consistent with the expected weakening of the trans effect upon protonation of the μ-oxo bridge. The weakening of antiferromagnetic coupling upon this protonation also greatly increases the paramagnetism of the clusters, which explains why all of the corresponding resonances are shifted substantially farther downfield and broadened compared to those of the μ-oxo bridged complexes. The magnetic properties of these hemerythrin diiron site models will be reported elsewhere.[14]

The magnesium-containing binuclear iron cluster, $[Fe_2MgO(O_2CMe)_6(N\text{-MeIm})_3]$, has the same "basic iron carboxylate" structure as does $[Fe_3O(O_2CMe)_6(N\text{-MeIm})_3]^+$. The magnesi-

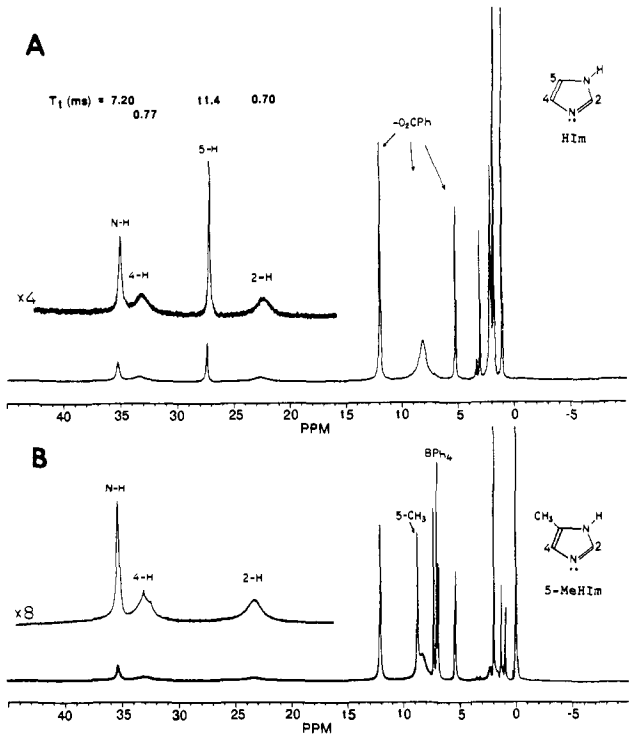

Figure 7. ^1H NMR spectra at 300 K in CD_3CN of (A) $[Fe_3O(O_2CPh)_6(HIm)_3]BF_4$ and (B) $[Fe_3O(O_2CPh)_6(5\text{-MeIm})_3]BPh_4$. ^1H T_1 values in milliseconds are listed above each imidazole resonance.

um–diiron(III) cluster has an effective magnetic moment of 2.38 μ_B/Fe, compared to 3.34 μ_B/Fe for the triiron(III) cluster. The relative paramagnetism of these two clusters is reflected in the imidazole ligand ^1H NMR resonances, which are all less shifted for $[Fe_2MgO(O_2CR)_6(Im)_3]$ (Table I). The assignments in Table I are for iron-bound imidazoles. The imidazoles bound to Mg in the solid salt do not appear in the NMR spectrum at 300 K, apparently due to exchange with solvent and/or free ligand. Rapid exchange is not evident for the iron-bound imidazole resonances, whose line widths and chemical shifts vary little with temperature between 300 and 240 K. This observation is consistent with the small change in molar susceptibility of $[Fe_2MgO(O_2CMe)_6(py)_3]$ over this temperature range.[19]

Figure 7 contains ^1H NMR spectra of the trinuclear high-spin ferric clusters, $[Fe_3O(O_2CPh)_6L_3]^+$ (L = HIm (A) and 5-MeIm (B)). These clusters have the "basic iron carboxylate" structure shown schematically in Chart I. In the case of $[Fe_3O(O_2CPh)_6(5\text{-MeIm})_3]^+$, the 5-methylimidazole, as opposed to the sterically less favorable 4-methylimidazole, coordination isomer was confirmed in solution by comparing the patterns of resonances in the region of imidazole ring protons to those of $[Fe_3O(O_2CPh)_6(HIm)_3]^+$. The pattern of resonances in Figure 7B, namely, two resonances with relatively short T_1's (at 23.3 and 32.7 ppm) and one resonance with a longer T_1 (at 35.3 ppm), confirms the 5-methyl coordination geometry. The 4-methyl coordination geometry would have a resonance pattern consisting of one shorter and two longer T_1's. Consistent with this analysis, the pairs of broader and narrower resonances are *both* present in the spectrum of $[Fe_3O(O_2CPh)_6(HIm)_3]^+$. The 5-methyl coordination geometry in $[Fe_3O(O_2CPh)_6(5\text{-MeIm})_3]^+$ has also been confirmed by an X-ray crystal structure.[28] A pair of weak, sharp peaks overlap the 4-H resonance in Figure 7B but not in 7A; the higher-field peak in this pair disappears in the presence of D_2O. These weak resonances are assigned to the N-H and 5-H protons of the 4-methylimidazole coordination isomer that is apparently present in a very small proportion.

The observability of imidazole ligand 2-H and 4-H resonances in spectra of the triiron(III) clusters is in contrast to spectra of the mononuclear and binuclear high-spin ferric complexes listed in Table I. This observation cannot be due solely to the reduced paramagnetism of the iron atoms in the trinuclear clusters, since the molar susceptibility per iron atom is greater for the trinuclear than the binuclear ferric clusters listed in Table I. Instead this observation indicates an unusually short T_{1e} for the triiron(III) clusters. Increasing the number of spin levels through magnetic coupling can increase the number of electron-spin relaxation pathways, thereby shortening T_{1e}.[29] For high-spin ferric complexes, T_{1e} has also been shown to be inversely proportional to the square of the axial zero-field splitting parameter, D.[2c,3b] Large values of D ($\gtrsim 5$ cm^{-1}) in high-spin ferric complexes should induce dipolar contributions to the isotropic shifts.[3a,30] However, the isotropic shifts in ppm for $[Fe_3O(O_2CR)_6(HIm)_3]^+$, namely, N(1)-H, 26.2; 4-H, 25.1; 5-H, 19.3; 2-H, 15.0, closely approximate the relative shifts expected for exclusively contact contributions through the σ system of imidazole.[31] In addition, the linear and nearly parallel temperature dependences of all isotropic shifts of $[Fe_3O(O_2CMe)_6(N\text{-MeIm})_3]^+$ (not shown) indicate that dipolar contributions are either small or nonexistent. We, therefore, conclude that the relatively short T_{1e} of $[Fe_3O(O_2CR)_6L_3]^+$ is due predominantly to the relaxation pathways provided by its eight spin levels ($S = {}^1/_2$ to ${}^{15}/_2$) and 216 spin states.[32]

Table III. ^1H NMR Chemical Shifts of Bridging Acetate Ligands in Tribridged High-Spin Iron(III) Clusters

complex	μ_{eff}/Fe,[a] μ_B	$-J$,[b] cm^{-1}	δ_{OAc},[c] ppm
$[(HB(pz)_3Fe)_2O(O_2CMe)_2]$	1.71[d]	122[d]	10.5[d]
$[Fe_2MgO(O_2CMe)_6(py\text{-}d_5)_3]$	2.39[e]	62[e]	13.4
$[Fe_3O(O_2CMe)_6(N\text{-MeIm})_3]^+$	3.34	30[f]	30.7
$[(HB(pz)_3Fe)_2(OH)(O_2CMe)_2]^+$	4.42[g]	17[g]	68.7[g]
$[(hxta)Fe_2(O_2CMe)_2]^-$	[5.06][h]	10[h]	89[h]

[a] Effective magnetic moments per iron atom at ~300 K from this work unless otherwise noted. [b] Values are listed for the $\hat{H}_{ex} = -2JS_1 \cdot S_2$ formalism. [c] Chemical shift at ~300 K of acetates that bridge two iron atoms, from this work unless otherwise noted. [d] Reference 38. [e] Reference 19. [f] From ref 39 for $[Fe_3O(O_2CMe)_6(H_2O)_3]^+$. [g] Reference 40. [h] Reference 33; magnetic moment was calculated from $-J$.

Bridging Acetate Resonances. Table III lists the observed chemical shifts of bridging acetate resonances in a series of binuclear and trinuclear high-spin ferric clusters in which the iron atoms are bridged by two acetates plus an oxo, hydroxo, or phenoxo ion. The observed downfield isotropic shifts are consistent with spin delocalization through the π system of the bridging bidentate carboxylate.[33] The bridging acetate chemical shifts vary monotonically with the effective magnetic moments per iron atom and with the pairwise antiferromagnetic coupling constants, J, in these complexes. The data in Table III confirm a previous correlation of this type[33] and extend it to the trinuclear "basic iron carboxylate" clusters. Due to differences in hyperfine coupling constants for the various spin levels in these complexes, a *linear* correlation between isotropic shift and magnetic coupling (expressed as μ_{eff}^2/Fe) is neither expected nor observed. However, Table III serves as a useful guide for setting limits on the extent of magnetic coupling in similar complexes. For example, the chemical shifts of the bridging acetates in the hemerythrin diiron(III) site models $[Fe_2O(O_2CMe)_2(TMIP)_2]^{2+}$ (10.1 ppm) and $[Fe_2(OH)(O_2CMe)_2(TMIP)_2]^{3+}$ (65.9 ppm) translate to $-J \gtrsim 122$ cm^{-1} and $-J \gtrsim 17$ cm^{-1}, respectively, according to Table III. The resonances of $[Fe_2O(O_2CMe)_2(TMIP)_2]^{2+}$ and $[Fe_2$-

(28) Wu, F.-J.; Kurtz, D. M., Jr.; Holt, E. M., unpublished results.

(29) (a) Banci, L.; Bertini, I.; Luchinat, C.; Scozzafava, A. *J. Am. Chem. Soc.* **1987**, *109*, 2328–2334. (b) Reference 24, pp 77–79.

(30) Behere, V.; Birdy, R.; Mitra, S. *Inorg. Chem.* **1982**, *21*, 386–390.

(31) The expected relative contact shifts are based on proton spin densities at each imidazole ring position from a CNDO calculation.[3c,27]

(32) Martin, R. L. In *New Pathways* in *Inorganic Chemistry*; Ebsworth, E. A. V., Maddock, A. G., Sharpe, A. G., Eds.; Cambridge University Press: London, 1968; pp 173–231.

(33) Arafa, I. M.; Goff, H. M.; Davis, S. S.; Murch, B. P.; Que, L., Jr. *Inorg. Chem.* **1987**, *26*, 2779–2784.

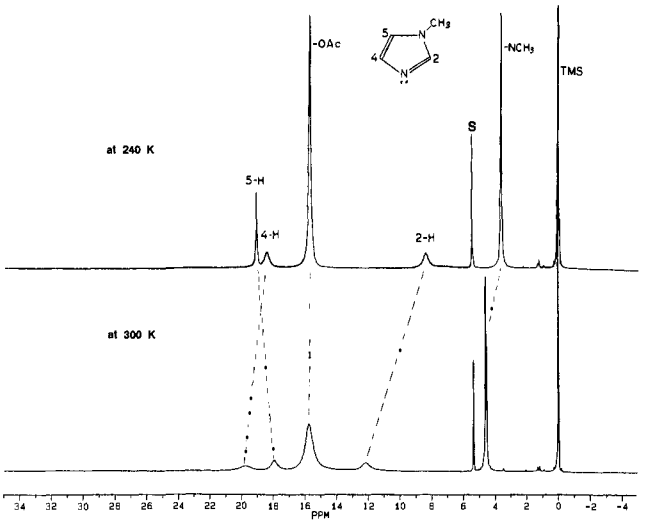

Figure 8. ^{1}H NMR spectra in CD_2Cl_2 of $[Fe_3O(O_2CMe)_6(N\text{-MeIm})_3]$ at 240 K (upper) and 300 K (lower). OAc = acetate; S = solvent.

$(OH)(O_2CMe)_2(TMIP)_2]^{3+}$ show *anti*-Curie and Curie behavior, respectively, between 300 and 240 K. This opposite temperature behavior parallels that expected for the magnetic susceptibilities of the two compounds, given the limiting values of J listed above.[34]

The acetates that bridge magnesium and iron in $[Fe_2MgO(O_2CMe)_6(py\text{-}d_5)_3]$ resonate at 8.8 ppm compared to 13.4 ppm for the acetates that bridge the two iron atoms. These assignments are consistent with a previous observation of smaller isotropic shifts for terminal than for bridging acetate methyls in high-spin ferric complexes.[33]

Mixed-Valent "Basic Iron Carboxylate" Clusters. All of the corresponding shifts of the mixed-valent trinuclear clusters are farther upfield than those of the triiron(III) clusters (cf. Table I and Figure 8). We attribute this phenomenon to three effects. First, the Evans susceptibility measurements for mixed-valent $[Fe_3O(O_2CMe)_6(N\text{-MeIm})_3]$ (cf. Experimental Section) show an ~17% reduction in molar susceptibility compared to the triiron(III) clusters. Second, smaller hyperfine coupling constants are expected in the mixed-valent cluster due to slight expansions in the coordination spheres caused by introduction of ferrous character. Third, the anti-Curie or non-Curie temperature dependences of the imidazole proton isotropic shifts (Figures 8 and 9) strongly suggest *upfield* dipolar contributions.[35]

The single acetate resonance of $[Fe_3O(O_2CMe)_6(N\text{-MeIm})_3]$ (Figure 8) is consistent with valence delocalization on the NMR time scale in solution. Mössbauer[17,36] and infrared[37] spectral data on the mixed-valent triiron clusters have been interpreted in terms of rapid intramolecular electron transfer between the iron atoms at 300 K. This "itinerant" electron apparently generates the principal magnetic susceptibility axis, which lies along the C_3 axis of the cluster.[36] We, therefore, measure dipolar contributions from the center of the *cluster* using eq 2. Comparison with the structure of the mixed-valent pyridine congener $[Fe_3O(O_2CMe)_6(py)_3]$[36] shows that all of the imidazole ligand hydrogens of $[Fe_3O(O_2CMe)_6(N\text{-MeIm})_3]$ lie well equatorial of the "magic angle" cone around the C_3 axis. Therefore, these hydrogens must have exclusively upfield dipolar contributions to their isotropic shifts. Assuming σ spin delocalization, the contact contributions to the imidazole isotropic shifts are exclusively downfield and should follow the pattern for the triiron(III) clusters. A downfield contact contribution is also expected for the bridging acetate CH_3.[33] The isotropic shift of this acetate methyl in $[Fe_3O(O_2CMe)_6(N\text{-MeIm})_3]$ has a relatively flat temperature dependence (Figure 9) because it lies near the "magic angle" (54.7°) and, therefore, has a relatively small dipolar contribution. From the atomic coordinates of $[Fe_3O(O_2CMe)_6(py)_3](py)$[36] we calculate $\theta = 53°$ for the acetate methyl carbon with respect to the center of the cluster. The contact contribution should parallel the molar susceptibility of $[Fe_3O(O_2CMe)_6(N\text{-MeIm})_3]$, which varies by less than 15% over the temperature range of Figure 9.[17b]

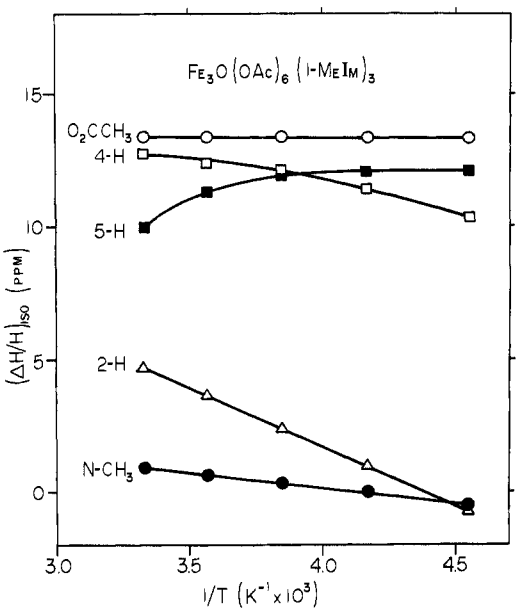

Figure 9. Temperature dependence of the isotropic shifts of $[Fe_3O(O_2CMe)_6(N\text{-MeIm})_3]$ in CD_2Cl_2.

The anti-Curie or non-Curie temperature dependences of the remaining isotropic shifts of Figure 9 indicate that upfield dipolar contributions, which contain a T^{-2} term, dominate the temperature dependence. The observation of a larger shift variation with temperature for the imidazole ligand 2-H than the 4-H (Figure 9) can be explained by the smaller contact contribution through the σ system of imidazole expected for the 2-H.[31] The 5-H lies at a relatively greater distance from the center of the cluster; therefore, the dipolar contribution for the 5-H must be smaller than for the 2-H and 4-H. The contact contribution for the 5-H is apparently sufficient to cause a net isotropic shift which decreases with temperature, although not linearly with T^{-1}. Similarly, the still greater distance of the N-CH_3 protons makes both the dipolar and contact contributions relatively small; a net anti-Curie temperature dependence is observed.

The 300 K shifts of $[Fe_3O(O_2CPh)_6(5\text{-MeIm})_3]$ listed in Table I probably represent the weighted averages for 5-methyl- and 4-methylimidazole coordination geometries. Below 270 K the spectra show evidence for both isomers in a respective ratio of ~5:1. As was observed for the triiron(III) clusters, the N(1)-H resonance is not the farthest downfield of the imidazole ring protons for the 4-methylimidazole coordination geometry.

At 240 K the line widths of the acetate methyl and benzoate ortho proton resonances are approximately 3 times narrower for the mixed-valent than for the triiron(III) "basic iron carboxylate" clusters, which implies a shorter T_{1e} for the former. This shortening is consistent with introduction of ferrous character into the cluster.

Conclusions and Implications for Non-Heme Proteins

^{1}H NMR of imidazole ligands in the various paramagnetic ferric and ferrous complexes are summarized below together with some implications for iron proteins. For approximations of histidyl

(34) Wojciechowski, W. *Inorg. Chim. Acta* **1967**, *1*, 319–324.

(35) We regard the possibility that a chemical equilibrium causes the differing temperature dependences of Figure 9 much less likely than dipolar contributions. The most likely chemical equilibrium, namely, ligand exchange with solvent, should cause all of the *N*-MeIm isotropic shifts to have temperature dependences in the same direction, which is contrary to observation. A similar argument can be made against intermolecular electron exchange. Other possible equilibria, e.g., parallel and perpendicular orientations of the imidazole ring with respect to the Fe_3 plane, or intramolecular electron transfer should cause broadening or splitting of the resonances at low temperature, once again contrary to observation.

(36) Woehler, S. E.; Wittebort, R. J.; Oh, S. M.; Kambara, T.; Hendrickson, D. N.; Inniss, D.; Strouse, C. E. *J. Am. Chem. Soc.* **1987**, *109*, 1063–1072.

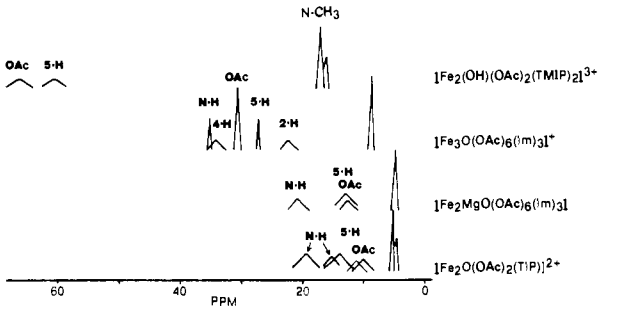

Figure 10. Schematic depiction of the dependence on antiferromagnetic coupling of ^1H chemical shifts and line widths for imidazole and acetate (OAc) ligands in high-spin ferric clusters. $-J$ increases from top to bottom (cf. Table III and text).

ligand chemical shifts, those of 5-methylimidazole usually provide the best comparison.

High-Spin Fe(II). The absence of appreciable dipolar contributions at 300 K for the effectively octahedral ferrous hexakis(imidazole) complexes means that the isotropic shifts calculated from the observed shifts in Table I can serve as contact shift references. For these complexes the order of isotropic shifts at 300 K is N(1)-H > 5-H > 4-H > 2-H > N-CH_3 ≳ 5-CH_3. The ^1H T_1's of the 2-H and 4-H are about an order of magnitude shorter than those of the 5-H and N-CH_3 and do not exhibit appreciable ligand-centered dipolar effects. A coordination environment of lower than octahedral symmetry induces dipolar contributions to the isotropic shifts, which in the case of $[Fe(N\text{-}EtIm)_6]^{2+}$ was detected by deviation of the 4-H resonance from Curie behavior at low temperature. The relatively short T_{1e} of high-spin Fe(II) means that, in addition to N(1)-H, the 2-H and 4-H resonances of histidine ligands could conceivably appear in ^1H NMR spectra of high-spin ferrous proteins. The narrowing of line widths due to a short T_{1e} is opposed in proteins by the broadening effect of a long rotational correlation time. The dinuclear high-spin ferrous site in deoxyhemerythrin and its anion adducts exhibit solvent exchangeable ^1H NMR resonances in the region 40–80 ppm that are assigned to N(1)–H of the five histidine ligands.[5] The range of chemical shifts is presumably due to variations in both the extent of antiferromagnetic coupling and dipolar contributions to individual isotropic shifts in the various derivatives. The ^1H NMR spectra of the azide, cyanate, and fluoride adducts of *P. gouldii* deoxyhemerythrin, in which the two high-spin ferrous ions are magnetically coupled to only a slight extent, exhibit broad nonexchangeable resonances in the region of 30 ppm.[5a] On the basis of our results, these resonances could be due to the 2-H and/or 4-H of histidine ligands. The chemical shift of the 5-CH_3 in $[Fe(5\text{-}MeIm)_6]^{2+}$, at 6.8 ppm, serves as an estimate of the histidine ligand β-CH_2 shift in the absence of dipolar contributions.

Low-Spin Fe(III). The well-established theoretical framework for analyses of isotropic shifts in heme proteins[3] can be applied quite satisfactorily to the low-spin ferric imidazole complexes examined in this work. Direct π spin delocalization leads to upfield contact contributions for imidazole ring protons and downfield contact contributions for ring methyls. Dipolar contributions can be either upfield or downfield, and, in the case of $[Fe(TICOH)_2]^{3+}$, these contributions were quantitatively separated (Table II). The results were used to determine the orientation of the imidazole rings with respect to magnetic axes, and by inference, molecular axes. These results coupled with the relatively short T_{1e} means that non-heme, low-spin ferric sites in proteins should be favorable candidates for ^1H NMR studies.

High-Spin Fe(III). Figure 10 schematically summarizes the chemical shifts and relative line widths of imidazole ligands for the high-spin ferric clusters examined in this work in the order of their paramagnetism. As expected, σ spin delocalization dominates, and the downfield isotropic shifts fall in the order N(1)-H > 4-H > 5-H > 2-H > 5-CH_3 ≳ N-CH_3. Evidence for the existence of a small proportion of the 4-methylimidazole coordination isomer was seen in spectra of $[Fe_3O(O_2CPh)_6(5\text{-}MeIm)_3]BPh_4$. In this case the N(1)-H resonance is not farthest downfield, and the appearance of a 5-H resonance farther downfield may, therefore, be characteristic of a histidyl coordination mode analogous to that of 4-methylimidazole.

It is clear from the cumulative results that the imidazole ligand 2-H and 4-H are generally not observable in high-spin ferric complexes, except in species with unusually short T_{1e}, such as the trinuclear "basic iron carboxylate" clusters. In fact, to our knowledge these trinuclear clusters represent the only example of a high-spin ferric complex where the imidazole ligand 2-H and 4-H resonances have been observed. Judging from the parallel behavior of the N-CH_3 and 5-CH_3 resonances, the histidyl ligand β-CH_2 should resonate well downfield of 10 ppm for magnetically uncoupled sites. In catechol 1,2-dioxygenase, which contains an isolated high-spin ferric ion, the histidyl ligand β-CH_2 has been assigned to resonances in the 20–40 ppm range.[2c] Our results indicate that for $-J \gtrsim 30$ cm^{-1} (the value for the trinuclear clusters), the β-CH_2 resonance will appear in the 2–9 ppm range. A monotonic correlation was found (Table III) between the extent of antiferromagnetic coupling and the chemical shift of the bridging acetate methyl resonance in these complexes. From Figure 10 the same trend is apparent for the imidazole resonances.

In ^1H NMR spectra of oxy- and azidomethemerythrin, a solvent nonexchangeable resonance at 11 ppm has been assigned to one or more of the α-methylene protons of the carboxylates that bridge the two iron atoms, and solvent-exchangeable resonances between 24 and 13 ppm have been assigned to N(1)-H of histidine imidazole ligands.[5] When compared with the protein spectra, the positions of both the acetate methyl (10.2 ppm) and N(1)-H (19.2 and 15.1 ppm) resonances in the μ-oxo-bridged hemerythrin diiron(III) site model, $[Fe_2O(O_2CMe)_2(TIP)_2](ClO_4)_2$ (Figure 6A), clearly confirm that oxyhemerythrin and azidomethemerythrin contain a μ-oxo rather than μ-hydroxo bridge. Due to the π spin delocalization pathway of the bridging carboxylates,[33] the isotropic shifts of the α-methylene or methyl protons will depend on the torsion angle, θ_H, between the C–H bond and the p_π orbital of the carboxylate carbon according to $\cos^2\theta_H$.[4b,23b] For restricted torsion angles, such as those of the methylenes in hemerythrin, this angular dependence can in principle give rise to isotropic shifts between zero and twice the averaged free-rotation value of the acetate methyl. Therefore, for the 11 ppm resonance in spectra of hemerythrin, only an approximate correspondence to the $-J$ values of Table III is expected. Given this caveat, the *combination* of acetate methyl and imidazole N(1)-H shifts for $[Fe_2O(O_2CMe)_2(TIP)_2]^{2+}$, $[Fe_2MgO(O_2CMe)_6(py\text{-}d_5)_3]$, and $[Fe_2MgO(O_2CPh)_6(HIm)_3]$ (Tables I and III), when compared to the analogous protein shifts,[5] leads to 62 cm^{-1} ≲ $-J$ ≲ 122 cm^{-1} for azidomethemerythrin.

The weighted average chemical shift of the four N–H resonances of azidomethemerythrin (assuming a 2:1:1:1 intensity ratio)[5] is 18.8 ppm, close to the weighted average chemical shift of 17.8 ppm for the two N(1)-H resonances of $[Fe_2O(O_2CMe)_2(TIP)_2](ClO_4)_2$. The 4.1 ppm separation between the latter two resonances reflects the μ-oxo trans effect. Constraints of the tridentate TIP ligand are likely to cause significant deviations from 90° and 180° angles expected for an octahedral coordination sphere and are also likely to impose a relatively uniform coordination geometry on the cis and trans imidazole ligands. These constraints will tend to minimize the trans effect of the μ-oxo bridge on the imidazole ligands.[37] (See note added in proof.) The absence of such constraints in the protein could contribute to the larger range of N–H resonances (24–13 ppm) observed in ^1H NMR spectra of oxyhemerythrin and azidomet-

(37) (a) Cannon, R. D.; Montri, L.; Brown, D. B.; Marshall, K. M.; Elliot, C. M. *J. Am. Chem. Soc.* **1984**, *106*, 2591–2594. (b) Meesuk, L.; Jayasooriya, U. A.; Cannon, R. D. *J. Am. Chem. Soc.* **1987**, *109*, 2009–2016.

(38) Armstrong, W. H.; Spool, A.; Papaefthymiou, G. C.; Frankel, R. B.; Lippard, S. J. *J. Am. Chem. Soc.* **1984**, *106*, 3653–3667.

(39) Dziobkowski, C. T.; Wrobleski, J. T.; Brown, D. B. *Inorg. Chem.* **1981**, *20*, 671–678.

(40) Armstrong, W. H.; Lippard, S. J. *J. Am. Chem. Soc.* **1984**, *106*, 4632–4633.

hemerythrin.[5] Of the five histidine imidazole ligands to the binuclear iron cluster in hemerythrin, two are trans and three are cis to the μ-oxo bridge.[41] The structure of highest resolution, that of azidometmyohemerythrin,[41b] shows that all three cis Fe-N_{Im} bond distances are more than 0.1 Å shorter than the two trans Fe-N_{Im} distances. μ-Sulfidomethemerythrin shows only two closely spaced N-H resonances (at 25 and 23 ppm),[5] consistent with the relatively smaller trans effect expected for a μ-sulfido bridge.

The best signature for a μ-hydroxo-bridged diiron(III) site in protein spectra may be histidyl ligand β-CH_2 resonances at $\sim$ 15-17 ppm, judging from the positions of the N-CH_3 resonances of $[Fe_2(OH)(O_2CMe)_2(TMIP)_2]^{3+}$ and $[Fe_2(OH)(O_2CEt)_2(TMIP)_2]^{3+}$ (Figure 6B).

(41) (a) Stenkamp, R. E.; Sieker, L. C.; Jensen, L. H. *J. Am. Chem. Soc.* **1984**, *106*, 618-622. (b) Sheriff, S.; Hendrickson, W. A.; Smith, J. L. *J. Mol. Biol.* **1987**, *197*, 273-296.

Mixed-Valent "Basic Iron Carboxylate" Clusters. All imidazole ring positions are observable. Because of valence delocalization, the opposing dipolar (upfield) and contact (downfield) contributions to the isotropic shifts can be understood by considering orientations and distances of the ligand protons with respect to the magnetic axes of the *cluster*.

Note Added in Proof. The X-ray crystal structure of $[Fe_2O(O_2CMe)(TMIP)_2](ClO_4)_2$ (Wu, F.-J.; Hagen, K. S.; Kurtz, D. M., Jr., unpublished results) shows that the two trans Fe-N_{Im} distances are an average of 0.03 Å longer than the four cis Fe-N_{Im} distances.

Acknowledgment. We thank Dr. Sergiu Gorun for a gift of TICOH, Jihu Zhang for experimental assistance, and Professor Larry Que, Jr., for helpful discussions. This research was supported by NIH Grant GM 37851 (D.M.K.). D.M.K. is an NIH Research Career Development Awardee.

Deuterium Isotope Effects on Carbon-13 NMR Shifts and the Tautomeric Equilibrium in *N*-Substituted Pyridyl Derivatives of Piroxicam

Jon Bordner, Philip D. Hammen, and Earl B. Whipple*

Contribution from Pfizer Inc., Central Research, Groton, Connecticut 06340.
Received January 5, 1989

Abstract: *N*-Alkylated pyridyl derivatives of piroxicam are formally zwitterionic but can, at the expense of aromaticity in the pyridyl ring, revert to neutral structures by means of fast internal proton transfers. The large change in dipole moment accompanying these tautomeric shifts makes the equilibrium unusually sensitive to changes in chemical substitution, solvent, and temperature. This property is used to formulate, test, and verify a new type of deuterium isotope effect on carbon-13 NMR shifts recently proposed by Hansen and, in the process, establish close correspondence with the general theory of isotope effects on proton transfer equilibria.

1. Introduction

In addition to being an important article of commerce as a nonsteroidal antiinflammatory agent,[1] piroxicam (Feldene) is an intrinsically interesting chemical compound by virtue of possessing four different heteroatom sites for positioning the two substituents necessary to complete its partial structure shown in Figure 1. Twelve isomers are possible if the substituents are nonidentical, and several have been prepared.[2] These differ remarkably in properties, particularly if substitution occurs on the pyridyl nitrogen to present the system with the formal alternatives of charge separation or bond localization in the pyridyl ring. Nevertheless, such substitution occurs with surprising ease.[2] When the amide nitrogen is also substituted, its fully valence-bonded structures are necessarily zwitterionic; yet piroxicam itself has been shown to crystallize in this form.[3] There is also, within the manifold of near-planar arrangements (which generally occur if one of the substituents is hydrogen), a total of eight possible geometrical isomers about the three partial double bonds connecting the two ring systems, and four of these arrangements (the 9,10 bond is consistently *Z*) have been found.

Piroxicam. The parent compound in which both substituents are hydrogen crystallizes in two forms, one of which has the initially proposed 7,10 *EZE* structure, **1a**,[4] and the other is a crystal hydrate of the zwitterionic 10,16 *ZZZ* form, **1b**.[3] It was

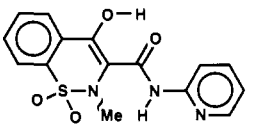

1a

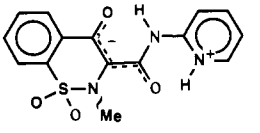

1b

recently demonstrated that the zwitterion coexists in equilibrium with the neutral form to the extent of 19% in *N*,*N*'-dimethylformamide (DMF) at 205 K, and the situation can be roughly extrapolated to include other polar solvents (e.g., DMSO) at ambient temperature.[5]

Monoalkyl Derivatives. The original attempts at *O*-methylation of piroxicam led instead to the *N*-methylated pyridyl derivative, and a series of *N*-alkyl homologs have since been reported.[2] Their physical properties (high melting points, yellow color, and low solubility) resemble zwitterionic piroxicam, and the crystal

(1) Lombardino, J. G.; Wiseman, E. H. *Med. Res. Rev.* **1982**, *2*, 127.
(2) Hammen, P. D.; Berke, H.; Bordner, J.; Braisted, A. C.; Lombardino, J. G.; Whipple, E. B. *J. Heterocycl. Chem.* **1989**, *26*, 11.
(3) Bordner, J.; Richards, J. A.; Weeks, P.; Whipple, E. B. *Acta Crystallogr.* **1984**, *C40*, 989.
(4) Kojic-Prodic, B.; Ruzic-Toros, Z. *Acta Crystallogr.* **1982**, *B38*, 2948.
(5) Geckle, J. M.; Rescek, D. M.; Whipple, E. B. *Magn. Reson. Chem.* **1989**, *27*, 150.

0002-7863/89/1511-6572$01.50/0 © 1989 American Chemical Society